Available online at www.sciencedirect.com
SCIENCE DIRECT®
Journal of Solid State Chemistry 177 (2004) 202–206
JOURNAL OF SOLID STATE CHEMISTRY
http://elsevier.com/locate/jssc

Crystallization of amorphous colloids: an effective approach for the rapid and large-scale preparation of antimony sulfide dendrites

Xuebo Cao, Yi Xie,* and Lingyin Li

Structure Research Laboratory, Department of Chemistry, University of Science and Technology of China (USTC), Hefei Anhui 230026, China

Received 26 May 2003; received in revised form 5 July 2003; accepted 12 July 2003

Abstract

Without the assistance of any templates and organic additives, orthorhombic antimony sulfide (Sb_2S_3) dendrites were obtained rapidly (3 h) through the crystallization of amorphous colloidal microspheres. The top view of dendrites reveals that their side branches are tetragonal prisms with a smooth face and nearly uniform breadth. The investigations on the growth mechanism demonstrated that the intermediate steps in the formation of dendrites are the rods and the structures with tip splitting. The kinetics of crystal growth, the anisotropic crystal structure and H^+ ions in the solution are believed to be responsible for the tip splitting. The structures with tip splitting subsequently grew and developed into dendrites eventually. A prolonged crystallization time (10 h) was found to be unfavorable to the further increase of dendrite size but led to its fragmentation.
© 2003 Elsevier Inc. All rights reserved.

Keywords: Fractal growth; Dendrites; Crystallization; Antimony sulfide; Morphologies

1. Introduction

Recently, much effort has been devoted to the control of the morphology and architecture of the inorganic substances with nano- to macroscopic-scale dimensions due to their fundamental and technological importance [1]. Compared with the size control, the morphology control is much more difficult, although their wires [2], plates [3], tubules [4], dendrites [5], cubes [6], and stars [7] have been obtained by various strategies. Of these shapes, fractal patterns are particularly attractive. Studying their formation provides a natural framework for the disordered system because fractals are generally observed in far-from-equilibrium growth phenomena [8]. In addition, the interests are greatly motivated by the fact that fractal growth phenomena are closely related to many processes of practical importance [9].

Various fractal structures, including dendrites [10], funnel-like structures [11], and the hierarchical structure with six-, four- and two-fold symmetries [12], can be prepared by a vapor transport and condensation technique or wet chemistry approaches. Most of synthesis strategies involved the use of hard templates or organic additives. The channels or pores in the hard templates limit the expansion of the crystal lattice; therefore, the features of the hosts determine the morphology and architecture of the products. Organic additives have the propensity to self-assemble into superstructures and thus they can function as crystal modifiers to direct the nucleation and anisotropic growth from the solution and allow for the generation of controlled morphologies and architectures. But the removal of templates and organic additives by acid, alkali or solvents is laborious, and the structures of the products are prone to be destroyed in the treatment process. Generally, although the templates or organic additives are necessary in much research, a large amount of fractal structures formed in natural world (e.g., snowflakes) do not need their direction and control. According to the theories for interpreting fractal growth phenomena, such as diffusion-limited aggregation (DLA) model [13] and cluster–cluster aggregation (CCA) model [14], the essential requirement is the formation of aggregates or crystals from small sub-unit-like atoms and colloidal particles that gradually develop into one crystal with a fractal pattern.

The direct crystallization of amorphous precursors seems to be an alternative strategy instead of the templates or additives for the morphology control of

*Corresponding author. fax: +865513603987.
E-mail address: yxielab@ustc.edu.cn (Y. Xie).

0022-4596/$ - see front matter © 2003 Elsevier Inc. All rights reserved.
doi:10.1016/S0022-4596(03)00401-8

inorganic substances. Previously, crystallization method was mainly used to improve the mechanical strength of alloys or the behaviors of magnetic materials [15], but a little of work directly used the crystallization method as an effective tool to control the morphologies of inorganic materials. It is well known that most of the amorphous colloids have a strong transformation tendency from thermodynamically metastable amorphous state to stable crystalline state under appropriate conditions. As for the crystalline products with a high anisotropic crystal structure, the crystallization is generally accompanied with the formation of desired structure due to the necessity to obtain a match between the symmetry of the crystal and their geometric shape [16,17].

The successful synthesis of antimony sulfide (Sb_2S_3) dendrites in the present paper verifies the feasibility of crystallization method. Usually, the direct precipitation from aqueous solution obtains orange amorphous Sb_2S_3, which has a strong tendency to form a gray orthorhombic modification of greater density at an elevated temperature (about 470 K) [18]. The transformation from the isotropic amorphous state to the intrinsically anisotropic orthorhombic phase can produce the Sb_2S_3 dendrites readily.

2. Experimental section

All the reagents are of analytical grade (Shanghai Chemical Reagents Co.) and used as received. In a typical experiment, analytical grade $SbCl_3$ (0.0002 mol) was dissolved in 5 mL analytical grade hydrochloric acid (36 wt%) at ambient temperature, and then it was diluted to 45 mL with distilled water under magnetic stirring to give a homogeneous solution. Afterward, the temperature was increased to 50°C and the solution was mixed with stoichiometric thioacetamide (0.0003 mol), which rapidly resulted in the formation of orange colloidal solution. This solution was transferred into a Teflon-lined stainless-steel autoclave (WeiBa, Shandong in China) with a volume of 50 mL. The sealed autoclave was allowed to maintain at 180°C for 3 h, then cooled down to ambient temperature. The resulted gray product was filtered and washed with the solution of tartaric acid and distilled water to remove the possibly remaining Sb^{3+} and any other impurities, and finally dried in vacuum at 60°C for 5 h. The products with a crystallization time of 10 min, 30 min, and 10 h at 180°C were also investigated.

The X-ray powder diffraction (XRD) patterns of the products were recorded on a Japan Rigaku D/max-γ rotation anode X-ray diffractometer (Cu$K\alpha$, $\lambda = 1.54178$ Å). The TEM images were taken with a HITICHAI H-800 electron microscope, using an accelerating voltage of 200 kV. High-resolution TEM (HRTEM) images and electron diffraction pattern were taken with a JEOL-2010 high-resolution electron microscope with an accelerating voltage of 200 kV. Specimens were prepared by spreading a drop of the ethanol suspensions onto copper grids coated with a thin amorphous carbon film and allowed to dry in air. The FESEM images were taken with a JEOL-JSM-6700F field emitting scan electron microscope (FESEM). FESEM samples were prepared by spreading the ethanol suspensions onto the copper sheet and sputter-coated with about 5 nm of gold.

3. Results and discussion

In our experiment, addition of thioacetamide into the $SbCl_3$ solution results in the formation of orange colloids immediately at a slightly elevated temperature (50°C). The typical X-ray diffraction (XRD) pattern of the orange Sb_2S_3 colloids is shown in Fig. 1a. No obvious peaks exhibit in the pattern at the 2θ range of 10–70°, indicating its amorphous characteristics. When it was treated in a hydrothermal environment for 3 h, the color of the product turns into gray and its XRD pattern is shown in Fig. 1b. The sharp and strong diffraction peaks indicate the high crystallinity of the products. All the reflections could be indexed to the orthorhombic Sb_2S_3 phase with lattice parameters $a = 11.227$ Å, $b = 11.318$ Å, and $c = 3.841$ Å, which are in good agreement with the reported data [19].

The crystallization time of amorphous Sb_2S_3 of only 3 h can produce its fractal pattern with the yield higher than 95%. Fig. 2 shows the typical FESEM images of the Sb_2S_3 fractal structure at low, medium, and high magnifications, respectively. The low-magnification image in Fig. 2a demonstrates clearly the large quantity of the fractal structure (dendrite). Its self-similarity can be

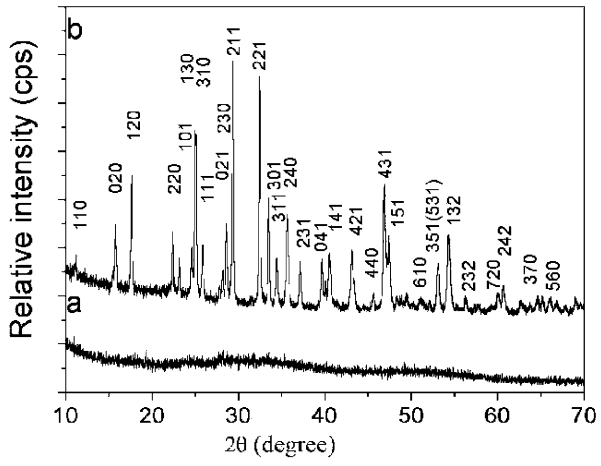

Fig. 1. XRD patterns of (a) orange Sb_2S_3 colloids and (b) the product with a crystallization time of 3 h.

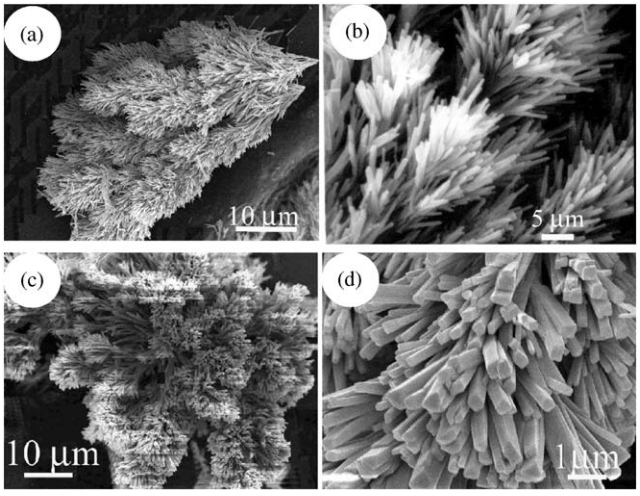

Fig. 2. Representative FESEM images of Sb_2S_3 dendrites made from the crystallization of amorphous Sb_2S_3. (a) A low-magnification image shows the dendritic pattern of the product. (b) A high-magnification image shows the side branches are uniform prisms. (c) The top view shows the three-dimensional similar feature of the dendrites. (d) A high-magnification of the top view reveals the prisms with a tetragonal face.

found easily in the medium magnification image as shown in Fig. 2b, from which one can see that the constitutive units of the side branches are large amounts of nearly uniform prisms with a radial spatial distribution. The high-magnification images (Figs. 2c and d) give further details about the fractal structure and the morphology features of the prisms. From the top view (Fig. 2c) one can learn that Sb_2S_3 dendrite has a three-dimensional self-similarity, which unlike the usual dendrites grows only along the two-dimensional direction [10–12,20]. The details about the prisms can be found in a partial-magnification image (Fig. 2d). Almost all the prisms have tetragonal and smooth end planes, which are well consistent with the crystal form of orthorhombic Sb_2S_3. Furthermore, the tetragonal and smooth end plane is significantly different from the side branches with an elliptic tip in most of the reported dendrites.

To reveal the intermediate steps in the transition from amorphous colloids to dendrites and the growth mechanism, the aliquots of Sb_2S_3 in the early stages of the dendrite formation were examined by transmission electron microscopy (TEM). The initial amorphous Sb_2S_3 colloids are composed of typical aggregates of spherical particles with an average diameter of 300 nm (Fig. 3a). The spherical feature of the products is consistent with the result of XRD because the isotropic nature of amorphous particles and the minimum surface tension determine their existence form of a spherical profile [21]. The electron diffraction pattern (inset in Fig. 3a) taken from these colloids also indicated that they were all in the amorphous phase. However, after crystallization at 180°C for 10 min, the rods with the

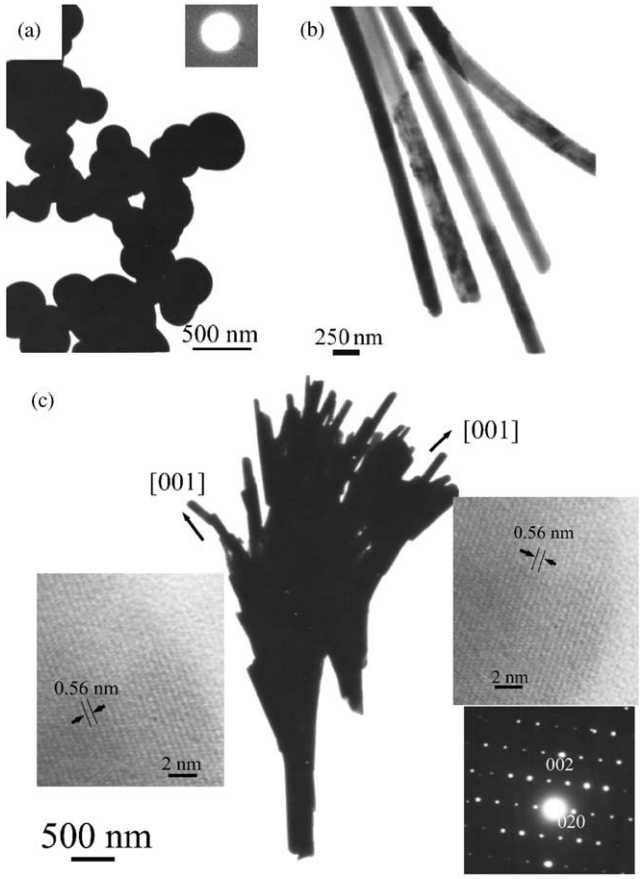

Fig. 3. TEM images of the intermediate state involved in the transition of amorphous colloids to dendrites. (a) Orange Sb_2S_3 is the aggregates of microspheres. The inserted ED pattern indicates their amorphous nature. (b) The rods appear in the products for the crystallization time of 10 min. (c) Tip splitting occurs with a crystallization time of 30 min; the typical HRTEM images and ED pattern are shown in the insets.

average breadth of 130 nm, as shown in Fig 3b, were observed in great abundance in the products. This result indicates that amorphous Sb_2S_3 can transform into low-dimensional crystals in a rather short time. When the crystallization time reaches 30 min, the tip splitting in the rod such as the ones presented in Fig. 3c would be observed. The studies of electron diffraction on the formed tips, such as the typical one in Fig. 3c, demonstrate that they are crystallized in the orthorhombic phase, and the longitudinal axis of all the tips is predominantly along the [001] direction, as marked by arrows in Fig. 3c. Lattice constants calculated from the diffraction pattern ($a = 11.224$ Å, $b = 11.315$ Å, and $c = 3.843$ Å) match well with the result of the XRD study and the reported data in the literature [19]. The single-crystalline nature and structure parameters were further confirmed by HRTEM images. Herein only two typical HRTEM images taken from different tips were presented in the inset of Fig. 3c. The fringe spacing

calculated from the HRTEM images was 0.56 nm and is well consistent with the separation between (020) planes of orthorhombic Sb_2S_3.

The rod and tip-splitting structure are presumed to be the intermediate states of spherical particle to dendrite transition. Although there are aggregates of colloidal particles in the system, as shown in Fig. 3a, no further experimental evidences can prove that the dendrites formed through the crystallization of the aggregates that fused gradually into one crystal. However, the rods and the subsequent tip splitting in Figs. 3b and c reveal that the point-initiated vectorial growth should be responsible for the formation of dendritic pattern. Considering that the growth process of Sb_2S_3 dendrites in the present experiment shares common characteristics with DLA growth model such as the ramified structure starting from an individual seed, the growth mechanism of the dendrites should be considered within the framework of DLA [13,22] as illustrated diagrammatically in Scheme 1.

Sb_2S_3 has a ribbon-like polymeric structure, in which each Sb atom and each S atom is bound to three atoms of the opposite kind, forming interlocking SbS_3 and SSb_3 pyramids [18]. This kind of molecular structure can confine and guide the one-dimensional growth along one particular axis, as has been demonstrated for selenium nanowires [23,24]. In addition, this occurs because the orthorhombic lattice is intrinsically anisotropic and has a unique (001) axis. The phase transition during the crystallization could cause the reorganization of crystal lattice and the formation of one-dimensional structure to obtain a match between the symmetry of the crystal and the uniaxial geometry of one-dimensional species [16]. As a result, the crystallization of amorphous colloidal particles leads to the formation of rods and this process can be facilitated by the low crystallization temperature of amorphous Sb_2S_3 (about 470 K) and the high pressure in the autoclave [18]. The driving force for the crystallization is the Gibbs free energy difference between the amorphous and the crystalline state [25]. According to the observation of TEM, a large amount of rods are found in the product with the crystallization time of 10 min. With the increase of crystallization time, the faces of the rods become rough and the tip splitting occurs, which is universal during the growth of dendrites [26]. Considering that dendrites have an extended surface and considerably increased surface free energy compared with the equilibrium shape of the crystal, it is thermodynamically unstable [9]. The origin of the tip splitting should result from the kinetics of crystal growth, which can be explained by the following facts. The diffusion of free Sb^{3+} and S^{2-} ions in the solution to the solid–liquid interface and the anisotropy of crystalline Sb_2S_3 allow the rods to grow along the preferred growth direction, which cause different growth rates at different sites on the rod tip [22]. Consequently, tip splitting occurs and brings about a dendritic pattern eventually. Additionally, since Sb_2S_3 is sensitive to acid, the erosion of Sb_2S_3 rods by H^+ ions in the solution will roughen the surface of the rods. Compared with the smooth rod faces, the rough rod faces are more favorable for the acceleration of the tip splitting and dendritic growth.

For the dendrites of Sb_2S_3, prolonging the crystallization time (up to 10 h) cannot cause the further increase of their size but leads to the destruction of dendritic patterns. FESEM observations find many side branches in the products and the images of the products with various magnifications are shown in Fig. 4. Their low-magnification FESEM images (Figs. 4a and b) demonstrate that almost all dendrites ruptured into advanced branches. High-magnification images (Figs. 4c and d) reveal the details of the side branches, from which one can learn that the end planes of the prisms are still tetragonal but their breadth is slightly smaller than what presented in Fig. 2e. It can be explained that dendrite is not the equilibrium shape of the crystal from the viewpoint of thermodynamics [9]. Consequently, the dendritic structure can be broken up to get the lowest energy. With the further increase of crystallization time, the advanced branches will fracture at the joints and the final products will be the single prismatic crystals, as reported in some previous research [27,28].

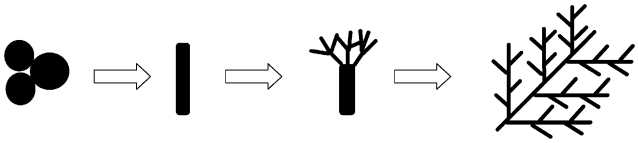

Scheme 1. Schematic description of the growth process of Sb_2S_3 dendrites.

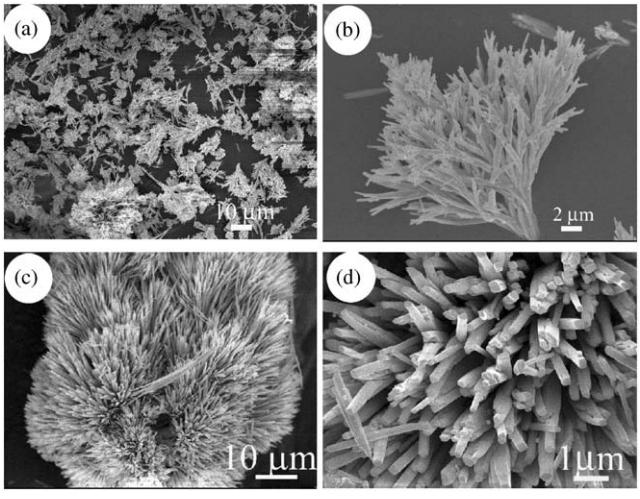

Fig. 4. FESEM images of the products with a crystallization time of 10 h. (a) A long crystallization time leads to the destruction of dendritic patterns. (b) A high-magnification image of the products. (c) A top view of the products. (d) A magnification image of the top view.

4. Conclusions

In summary, we report a simple convenient and efficient method for the morphology control of Sb_2S_3. Through the transition of the amorphous state to the highly anisotropic orthorhombic phase for only 3 h, Sb_2S_3 dendrites were obtained with the yield higher than 95%. And the growth of the dendrites did not need the participation of any templates and organic additives.

Furthermore, the growth mechanism is identified clearly through the investigations on the intermediate steps involved in the formation of Sb_2S_3 dendrites. The key steps in the transition of colloidal spheres to dendrites are found to be the rods with a diameter of 130 nm and the tip-splitting structures. A prolonged crystallization time is unfavorable to the further increase of dendrite size but lead to the destruction of fractal patterns.

We believe that this crystallization strategy will be applied in the production of most alloys, oxides, other sulfides and pure element systems with desired structures as long as these materials are highly anisotropic in crystal structures and can be prepared in the amorphous state.

Acknowledgments

Financial supports from National Natural Science Foundation of China, Chinese Ministry of Education and Chinese Academy of Sciences are gratefully acknowledged.

References

[1] D.D. Archibald, S. Mann, Nature 364 (1993) 430–433.
[2] X.G. Peng, L. Manna, W.D. Yang, J. Wickham, E. Scher, A. Kadavanich, A.P. Alivisatos, Nature 404 (2000) 59–61.
[3] S.H. Chen, Z.Y. Fan, D.L. Carroll, J. Phys. Chem. B 106 (2002) 10777–10781.
[4] J. Lu, Y. Xie, F. Xu, L.Y. Zhu, J. Mater. Chem. 12 (2002) 2755–2761.
[5] J.P. Xiao, Y. Xie, R. Tang, W. Luo, J. Mater. Chem. 12 (2002) 1148–1152.
[6] L.F. Gou, C.J. Murphy, Nano Lett. 3 (2003) 231–235.
[7] D. Volkmer, S. Tugulu, M. Fricke, T. Nielsen, Angew. Chem. Int. Ed. 42 (2003) 58–61.
[8] R. Trivedi, W. Kurz, Int. Mater. Rev. 39 (1994) 49–74.
[9] T. Vicsek, Fractal Growth Phenomena, 2 Edition, World Scientific, Singapore, 1992.
[10] J.P. Xiao, Y. Xie, R. Tang, M. Cheng, X.B. Tian, Adv. Mater. 13 (2001) 1887–1891.
[11] S.H. Yu, M. Antonietti, H. Cölfen, J. Hartmann, Nano Lett. (Asap article) (2002) A-D.
[12] J.Y. Lao, J.G. Wen, Z.F. Ren, Nano Lett. 2 (2002) 1287–1291.
[13] T.A. Witten, L.M. Sander, Phys. Rev. Lett. 47 (1981) 1400–1403.
[14] P. Meakin, Phys. Rev. Lett. 51 (1983) 1119–1122.
[15] K. Lu, Adv. Mater. 11 (1999) 1127–1128.
[16] Z.Y. Tang, N.A. Kotov, M. Giersig, Science 297 (2002) 237–240.
[17] B. Gates, B. Mayers, A. Grossman, Y.N. Xia, Adv. Mater. 14 (2002) 1749–1754.
[18] R.B. Heslop, K. Jones, Inorganic Chemistry: A Guide to Advanced Study, Elsevier Scientific Pub. Co., Amsterdam, 1976.
[19] JCPDS file, No. 6-474.
[20] Y. Zhou, S.H. Yu, C.Y. Wang, X.G. Li, Y.R. Zhu, Z.Y. Chen, Adv. Mater. 11 (1999) 850–852.
[21] C.D. Lokhande, B.R. Sankapal, R.S. Mane, H.M. Pathan, M. Muller, M. Giersig, V. Ganesan, Appl. Surf. Sci. 193 (2002) 1–10.
[22] S.Z. Wang, H.W. Xin, J. Phys. Chem. B 104 (2000) 5681–5685.
[23] B. Gates, Y.D. Yin, Y.N. Xia, J. Am. Chem. Soc. 122 (2000) 12582–12583.
[24] B. Gates, B. Mayers, B. Cattele, Y.N. Xia, Adv. Funct. Mater. 12 (2002) 219–227.
[25] K. Lu, Mater. Sci. Eng. R. 16 (1996) 161–221.
[26] U. Bisang, J.H. Bilgram, Phys. Rev. E 54 (1996) 5309–5326.
[27] Q. Yang, K.B. Tang, C.R. Wang, Y.T. Qian, W.C. Yu, G. Zhou, F.Q. Li, J. Mater. Chem. 11 (2001) 257–259.
[28] X.W. Zheng, Y. Xie, L.Y. Zhu, X.C. Jiang, Y.B. Jia, W.H. Song, Y.P. Sun, Inorg. Chem. 41 (2002) 455–461.